5.1 Use of Satellite Altimetry in Studies of the Oceanic Lithosphere

A. Cazenave[1] and E. A. Okal[2]

[1] *Groupe de Recherches de Géodésie Spatiale, Centre National d'Etudes Spatiales, Toulouse, France and* [2] *Department of Geological Sciences, Northwestern University, Evanston, Illinois, USA*

Introduction

ver the last decade, the collection of marine geoid data over all oceanic eas by the GEOS-3 and SEASAT altimeter satellites has triggered a newal of interest in the use of gravity information in marine geophysics, id has motivated a number of new studies of the oceanic lithosphere and per mantle. Several maps of the sea surface height have been produced i both global and regional scales, based either on GEOS-3, SEASAT or th datasets (e.g., Rapp, 1983; Marsh *et al.*, 1985, 1986). In order to obtain aps of the mean sea surface heights over a regular grid from individual

ICE GEODESY AND GEODYNAMICS
N 0-12-057840-9

satellite profiles, a number of interpolation methods are used after minimizing by least squares procedures the differences at altimeter profile intersections which result from inadequate orbital modeling (e.g. Balmino *et al.*, 1979; Marsh *et al.*, 1980; Rapp, 1983). The raw sea surface topography contains a component of oceanic origin (tides, currents, eddies, etc.), which is known to be less than 1 m in amplitude. Therefore, the sea surface maps closely represent the geoid, and can be used for investigations of density differences within the Earth. The so-called crossing arcs adjustment procedures, applied to remove orbital errors, also remove oceanographic effects so that the precision of the geoid surface approaches that of the measurements themselves, i.e. ~10–20 cm for SEASAT.

As we already know from global geopotential solutions derived from satellite orbit perturbations (e.g. Lerch *et al.*, 1981; Reigber *et al.*, 1985) the geoid is dominated by long anomalies with wavelengths of several thousand kilometers, poorly correlated to surface tectonic features, and usually attributed to density variations in the lower mantle or at the core–mantle interface. The marine geoid presented in Fig. 1 is one of the latest solutions obtained by Marsh *et al.* (1986) with SEASAT data over a $0.5° \times 0.5°$ grid, and confirms these characteristics. In addition, and unlike global geopotential solutions, the altimeter geoid clearly depicts numerous bathymetric features such as deep-sea trenches, volcanic chains or major fracture zones. In order to be used successfully for geophysical interpretation, these tectonic signatures can be enhanced by removing unrelated longer-wavelength geoid undulations; this is currently done by subtracting the cumulative long-wavelength contributions of a global geopotential field; since spherical harmonic expansion on a sphere is analogous to Fourier spectral expansion on a plane, each harmonic of degree n corresponds to a particular wavelength $\simeq 2\pi R/n$ (R being the Earth's radius). Subtracting a global geopotential field up to degree 10 from the altimeter geoid therefore provides a residual geoid surface with undulations of wavelength $\lambda < 4000$ km, on which tectonic signatures are now very apparent, as shown in Figs. 2 and 3.

As evidenced in Fig. 2, the main characteristic of the residual geoid is a clear three-dimensional pattern of geoid highs and lows, with typical wavelengths λ ~2000–3000 km and typical amplitudes 5–10 m. These undulations have been attributed to small-scale convection in the upper mantle (e.g. McKenzie *et al.*, 1980; Marsh *et al.*, 1984; Watts *et al.*, 1985). At smaller scales, marine geoid data offer important constraints on the physical structure of the oceanic lithosphere and have been extensively used in recent studies in addition to bathymetry, gravity, sea floor age, seismic or heat flow data. While it is well known that inversion of gravity for internal density distribution is highly non-unique, it appears that if tectonic structures are isostatically compensated (locally or regionally, statically or dynamically),

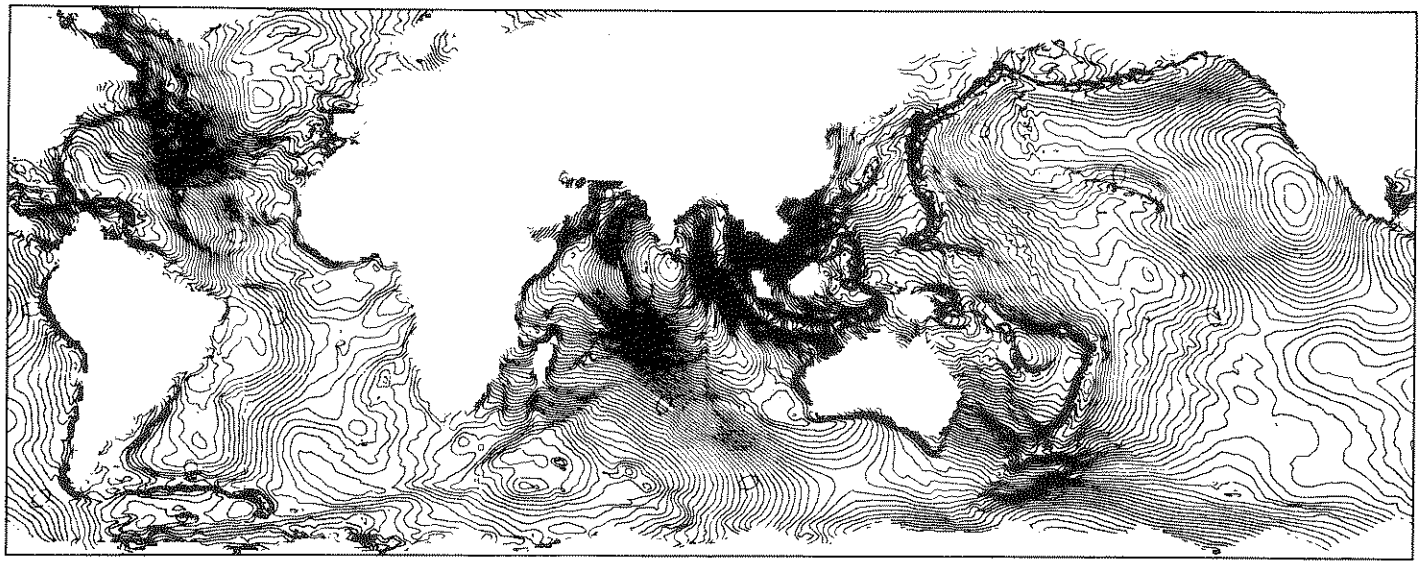

Fig. 1. Marine geoid derived from the SEASAT altimeter data. [After Marsh *et al.* (1985b).]

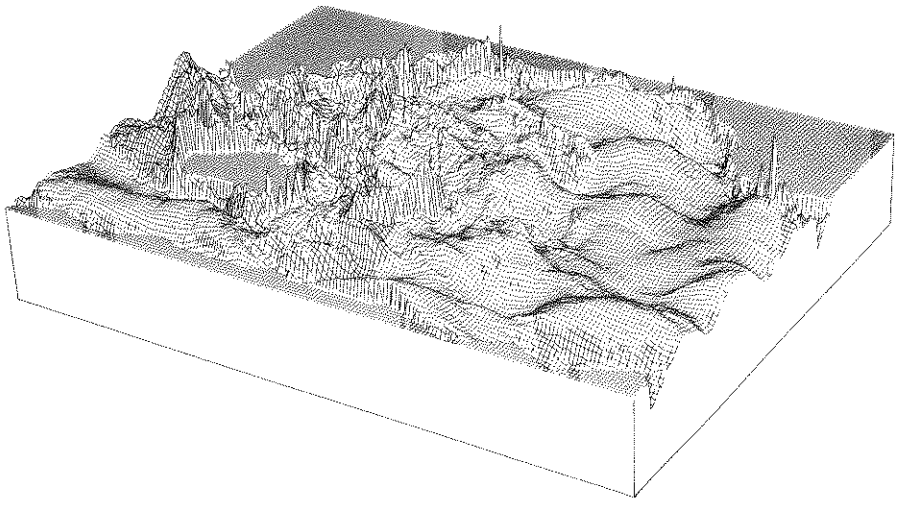

Fig. 2. Three-dimensional view of the geoid over the Pacific Ocean looking northeast, after removal of wavelengths greater than 4000 km.

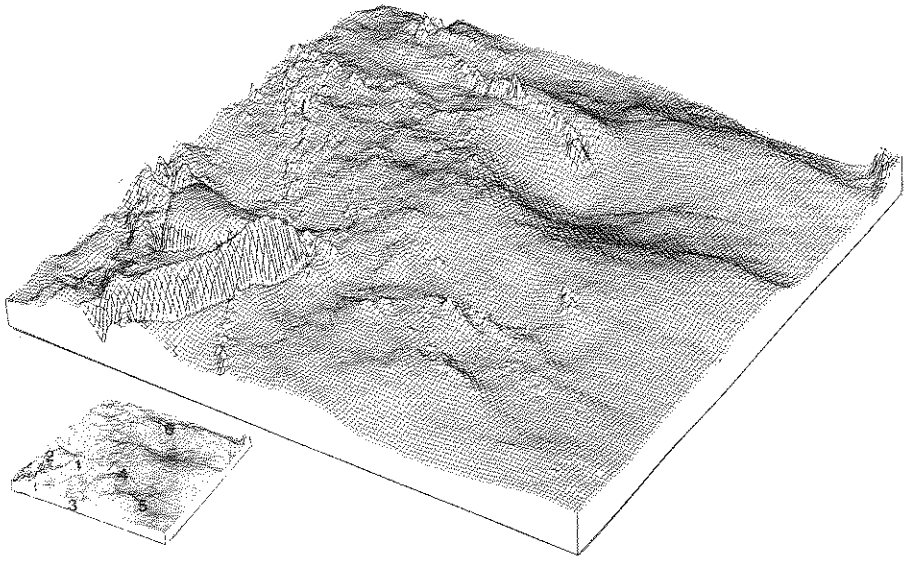

Fig. 3. Three-dimensional view of the geoid over a close-up section of the Pacific Ocean, after removal of the degree 10 geoid. Inset at lower left identifies: (1) Tonga Trench, (2) Vanuatu Trench, (3) Louisville Ridge, (4) Society Islands Chain (Tahiti), (5) Austral Islands Chain, and (6) Hawaiian Islands Chain.

the corresponding geoid anomalies give strong constraints on any proposed theoretical model. This results partly from the fact that each kind of tectonic feature gives a specific signature in the geoid; thus, on the basis of generally accepted models, analyses of the shape, amplitude and wavelength of the associated geoid anomalies can yield information on the internal density structure as well as on its state of isostatic compensation (e.g. Turcotte, Chapter 5.4). The following is a short description of the typical geoid signatures of a few major tectonic features.

1. Volcanic Chains and Isolated Seamounts

These give large positive geoid anomalies, up to 5–6 m amplitude and ~150-km wide, sometimes flanked by small adjacent minima (see Fig. 4). These anomalies result from two opposite effects: the positive geoid anomaly due to the topography and the negative anomaly due to its (often partial) isostatic compensation inside the lithosphere.

2. Symmetrically Spreading Ridges

Over symmetrically spreading ridges, the geoid height anomaly results from the cooling of the lithosphere and decreases from the ridge crest to old basins as sea floor age increases. Typical geoid height changes are 5–10 m over distances of 1000–2000 km. The observed shape of the geoid has been used as a constraint on the cooling models of the lithosphere or on the magnitude of the plates' driving forces (Sandwell and Schubert, 1980; Parsons and Richter, 1980). Figure 5 shows observed geoid height over the East Pacific Rise, decreasing away from the ridge crest with a symmetric behavior. In general, slow-spreading ridges, such as the Mid-Atlantic Ridge, have much stronger geoid signatures than fast-spreading ones, such as the East Pacific Rise.

3. Fracture Zones

Over fracture zones, geoid anomalies show a step-like signal of 1–3 m amplitude, downward from the younger, shallower side to the older, deeper side of the fracture zone. Figure 6 shows examples of this geoid step. It occurs because the portions of the plate on each side of the fracture zone have different thicknesses and density structures, as predicted by thermal models of the evolution of the oceanic lithosphere. Several analyses of geoid

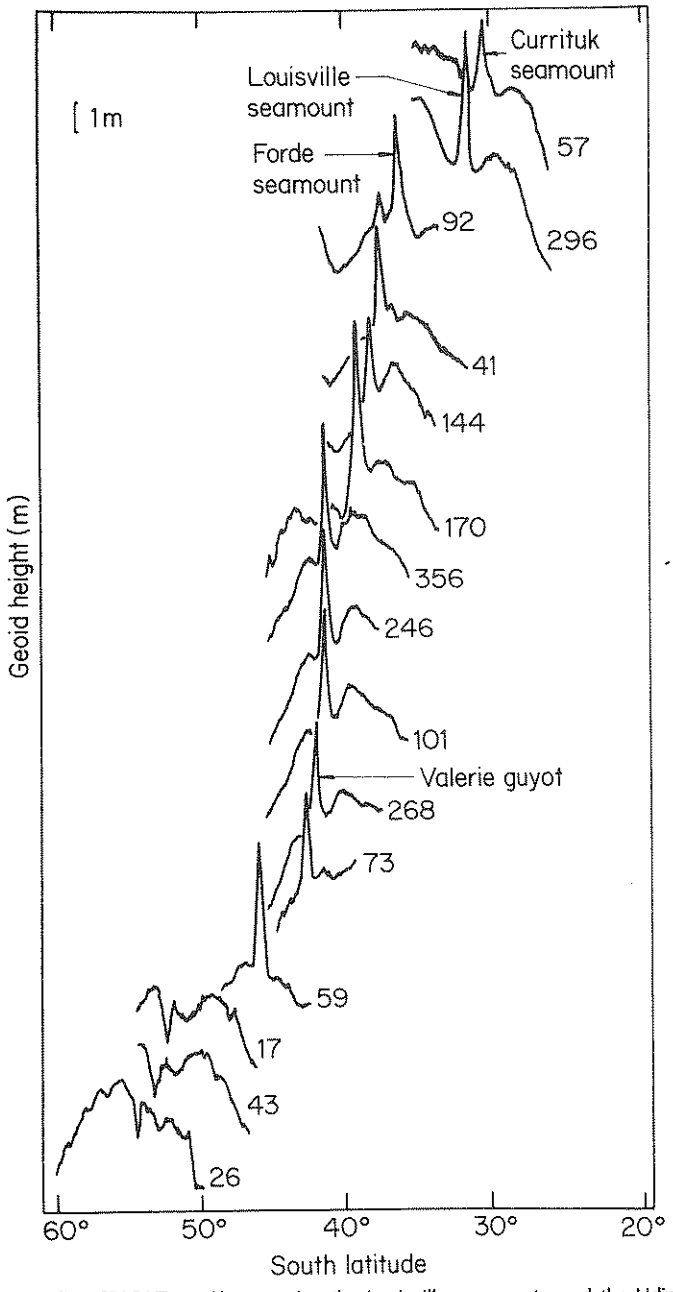

Fig. 4. Descending SEASAT profiles crossing the Louisville seamounts and the Udintsev and Tharp fracture zones. Geoid anomalies are in m: profiles are arranged by increasing southward latitudes.

Fig. 5. Geoid profiles across the East Pacific Rise. These are cross-sections perpendicular to the rise, which have been reconstructed from the three-dimensional SEASAT geoid computed over this region.

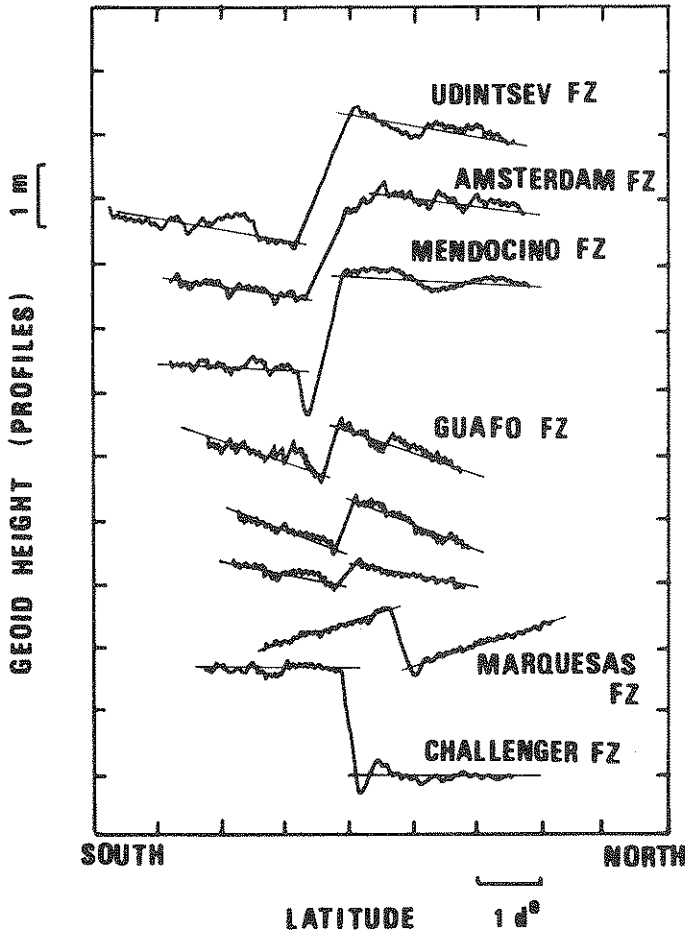

Fig. 6. SEASAT geoid profiles across a selection of fracture zones. Geoid offsets Δh are measured between the parallel solid lines.

anomalies at fracture zones have been conducted to estimate the parameters entering in the models of lithospheric cooling, as we will discuss in more detail in Section III.

4. *Deep-sea Trenches*

Deep-sea trenches also give rise to a typical geoid signature (Fig. 7). Directly over the trench axis, the geoid presents a narrow trough 5–20 m in depth

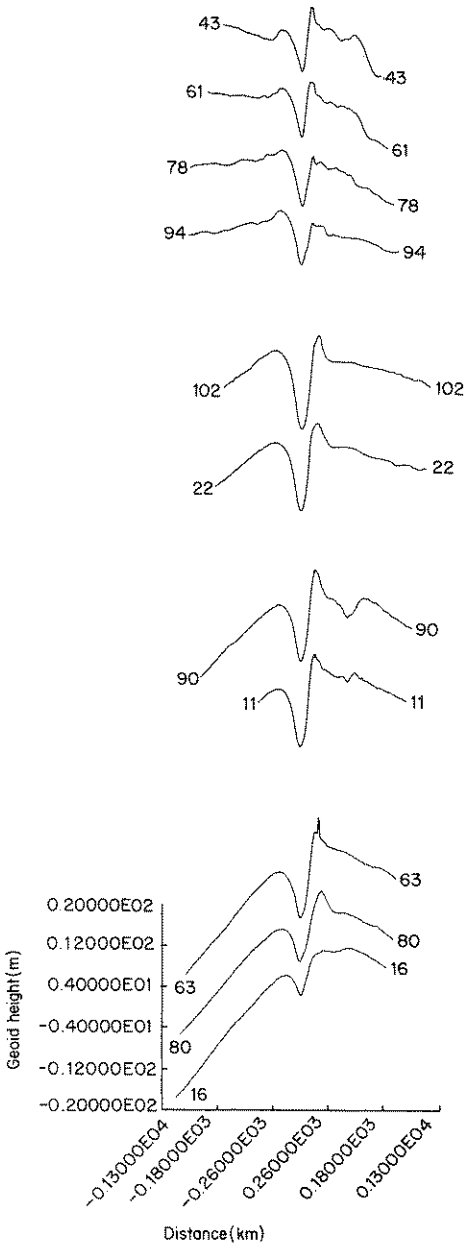

Fig. 7. SEASAT geoid profiles across the Aleutian subduction zone.

and 100–400 km in width. From the trench to the landward side, there is a steep increase coinciding generally with the island arc when present. Superimposed on this short-wavelength variation, one observes a broad positive anomaly in the geoid, starting 1000–3000 km away from the trench axis on the seaward side of the subducting plate. This long-wavelength geoid high reaches its maximum in the approximate vicinity of the trench and typical amplitudes vary from 10 m to a few tens of meters; because of the filtering procedure, it is absent on the residual geoid. Although differing in their detailed expression, all known subduction zones produce geoid anomalies with the above characteristic trends. Several studies have attempted to explain these anomalies; although interpretations differ in some details, there is a general agreement to ascribe the broad positive high to thermal effects associated with the cold, dense subducting slab penetrating the asthenosphere, while the short-wavelength geoid low results from the flexure and subduction of the plate at the trench axis. The observed asymmetry in the shape of the negative anomaly at the trench is due to flexure of the plate on the seaward side, which is also responsible for the occasional presence of an outer rise in the bathymetry.

5. Passive Continental Margins

Passive continental margins also produce a step-like geoid signature which is due in this case to a difference in crustal thicknesses between the continental and oceanic sides. Figure 8 illustrates an example of geoid profile across a continental margin.

Application of altimeter geoid data to marine geophysics have up to now been concentrated along two main avenues: (1) investigation of the rheology of the oceanic lithosphere and its thermal evolution and (2) prediction of bathymetry in uncharted areas. The following sections review some recent work in each of these domains.

II. Geoid Anomalies Over Seamounts: Lithospheric Flexure

We have seen that there exists a strong correlation between local geoid anomalies and the presence of seamounts on the ocean floor. Earlier studies over the Hawaiian islands (Vening Meinesz, 1941) had shown that such localized topographic features are regionally, rather than locally, compensated by lithospheric flexure. Later on, the mechanical response of the oceanic lithosphere to surface loads (such as isolated seamounts, volcanic island chains, sediments and ice sheets) or to bending stresses (in subduction

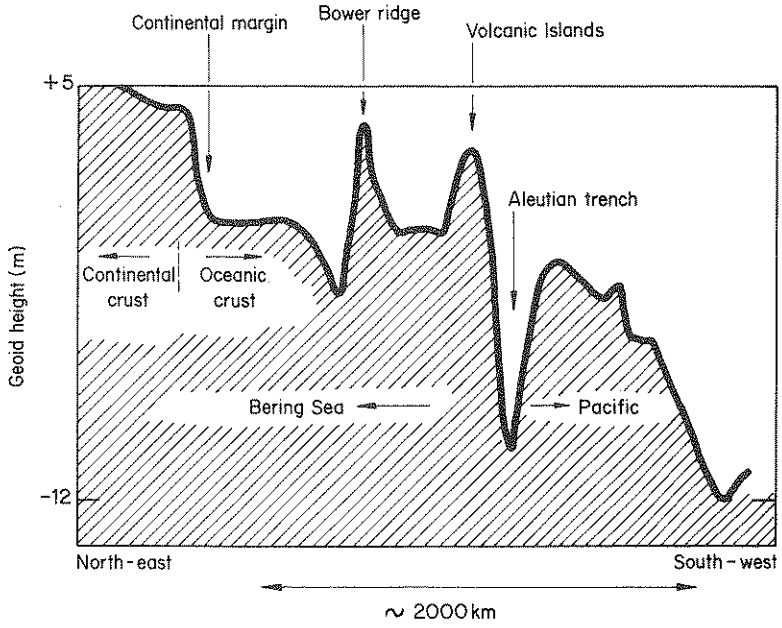

Fig. 8. SEASAT geoid profile across the Bering Sea continental margin.

areas) was studied extensively on the basis of simple models of elastic or viscoelastic flexure, by using data from bathymetry, uplift or subsidence, gravity and more recently, the geoid. The most widely applied model is the elastic one, based on the equilibrium theory of deformation of thin elastic loaded plates overlying a weaker fluid medium. The parameter that characterizes the flexure of the plate is the flexural rigidity D, related to the elastic thickness H by:

$$D = EH^3/[12(1-\nu^2)]$$

where E and ν are Young's modulus and Poisson's ratio, respectively.

The comparison of observed data (gravity, geoid height, uplift, etc.) with theoretical estimates allows the derivation of best-fitting values for D, and thus for H. Watts *et al.* (1982) compiled all available elastic thicknesses, estimated by various authors at different oceanic locations; they showed that the elastic thickness of the oceanic lithosphere increases linearly with the square root of the age of the plate at the time of loading, and concluded that the upper layer of the lithosphere is reasonably well described by an elastic rheology for geological time scales (see also Watts, 1978). Although

the elastic model seems to account very well for observations of loading by seamounts, other authors (e.g. Lambeck, 1981) prefer a viscoelastic model of the global response of the lithosphere to an applied load. In this case, the "equivalent" elastic thickness determined from the flexural response of the plate should decrease with the age of the load. We will not discuss this matter further as it is developed by Watts; we only wish to stress that the global coverage of altimeter data allows their systematic use (unlike marine gravity data) to study the flexural response of the oceanic lithosphere under surface loads, in order to test the range of validity of the simple elastic model (influence of the size of the load, of the tectonic environment, etc.).

III. Geoid Anomalies over Spreading Ridges and Fracture Zones: Thermal Evolution of the Oceanic Lithosphere

Two simple models of the thermal structure of the oceanic lithosphere have been proposed in order to explain cooling and contraction as the plate expands away from the ridge crest.

The first model, known as the half-space model, assumes that the cooling plate can be treated as a thermal boundary layer of a large-scale mantle convection cell (Turcotte and Oxburgh, 1967). The base of the plate is then defined as the solid–liquid phase boundary of the material, and thus follows an isotherm (Parker and Oldenburg, 1973; Oldenburg, 1975). A further assumption is the absence of lateral conduction in the plate. In this model, both plate thickness and depth to the seafloor increase linearly with the square root of age, while heat flow decreases as the inverse square root of age.

The second model, known as the plate model, assumes a plate of nearly constant thickness moving away from the ridge crest at a constant velocity. This kind of model was originally developed by McKenzie (1967) to account for heat flow observations, and several variations of the model have later been proposed (e.g. Bottinga, 1974; Bottinga and Allègre, 1976).

The two models predict almost the same behavior for depth to the seafloor, heat flow and geoid in young oceans, but in oceans older than about 70 Ma, the plate model predicts a general tapering of the cooling with depth to the seafloor and heat flow tending asymptotically toward a constant value. This asymptotic behavior is indeed generally observed in the older ocean basins, and thus the plate model is generally preferred to the half-space model. Figure 9 presents the observed ocean depth as a function of age (after Parsons and Sclater, 1977). The solid curve corresponds to the predicted variation in the case of the plate model while the

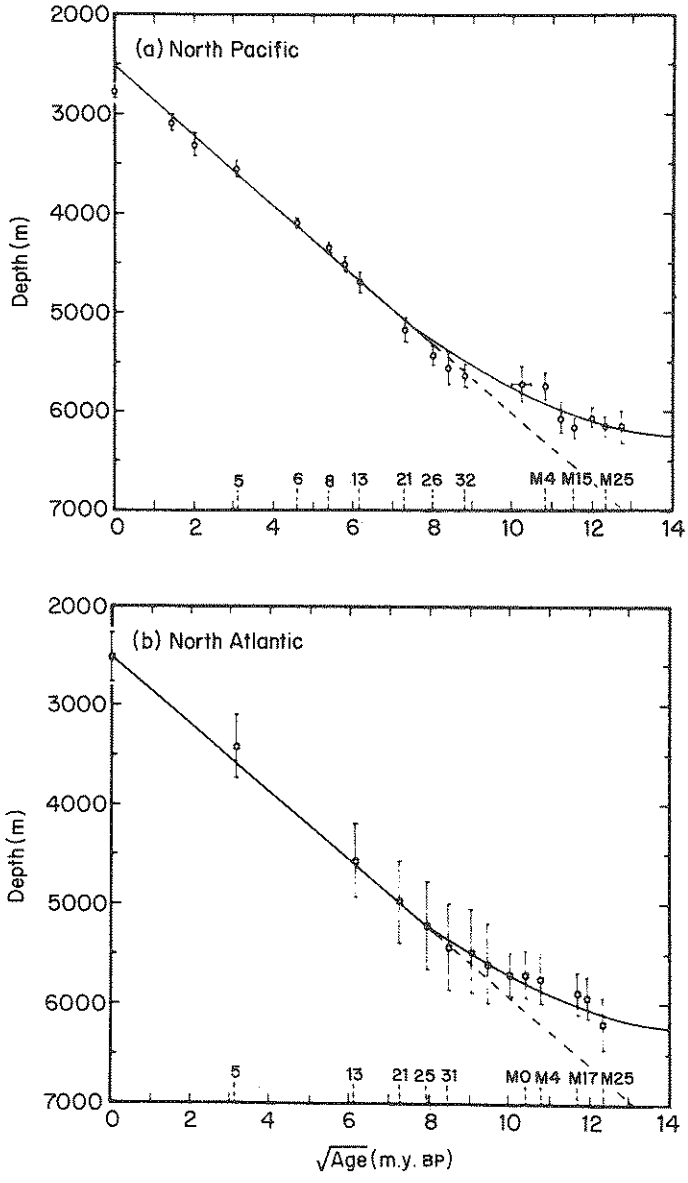

Fig. 9. (a) Plot of mean depth in the North Pacific versus square root of age. Numbers at bottom of the figure refer to selected Cenozoic and Mesozoic magnetic anomalies. (b) Same plot for the North Atlantic. Open circles with error bars give the mean depth and standard deviation, the solid curve gives the theoretical elevation for the plate model, and the dashed curves give the linear $t^{1/2}$ relation. [From Parsons and Sclater (1977).]

dashed curve corresponds to the half-space model. Clearly, the plate model fits the depth data better. This model requires an additional heat source in the mantle to counteract the thickening of the plate in older basins.

Tests of thermal models have traditionally been based on data from topography and heat flow [Sclater and Francheteau, 1970; Parsons and Sclater, 1977]. However, large areas of the ocean floor are either shallower or deeper than predicted by "normal" thermal subsidence, while available heat flow data are not always a sensitive discriminant of the two models. In particular, Heestand and Crough (1981) have argued that the tapering off of the bathymetry in older ocean basins (a major argument in favor of the plate model) could in fact be due to thinning, reheating and subsequent uplift of the lithosphere as it moves over hotspots; when corrected for this bias, they claim that oceanic lithosphere could follow the behavior predicted by the half-space model. Similarly, Wood and Yuen (1983) have proposed to interpret the relative uplift of the older lithosphere in the framework of the half-space model, by involving a change of mineralogy with a negative Clapeyron slope inside the plate.

Like heat flow and depth data, geoid data can in principle discriminate between the two thermal models: cooling of the lithosphere causes the geoid height to decrease with increasing plate age, symmetrically away from the ridge crest. The absolute change in geoid height with age, due to lithospheric cooling, is typically 5–10 m over distances of 1000–2000 km, and thus is difficult to isolate from other unrelated long-wavelength anomalies. On the other hand, at a fracture zone, there exists a strong discontinuity in plate age, resulting in a major short-wavelength geoid offset featuring a step-like signature, downward from the younger, shallower side to the older, deeper side, with amplitude ranging from a few tens of centimeters to a few meters over distances of only 100–150 km. The geoid offset Δh divided by the age offset Δt approximates the derivative with respect to age of the geoid height $h(t)$, due to lithospheric cooling. Thus, if the age of each side of the fracture zone is known, the observed dependence of $\Delta h/\Delta t$ on age can be used to compare the theoretical curves derived from cooling models, allowing some model parameters to be estimated.

We have analyzed geoid height data over many fracture zones of the Pacific Ocean (among others, the Mendocino, Udintsev, Menard, Marquesas, Challenger fracture zones). More than 15 different fracture zones have been considered and ~85 geoid offsets have been collected over a large area extending 60°S–40°N and 80°–160°W, and covering a range of plate ages of ~60 Ma. The quantity $\Delta h/\Delta t$ has been estimated and the observed dependence of $\Delta h/\Delta t$ on age has been derived. A semi-logarithmic plot of this relationship is shown in Fig. 10.

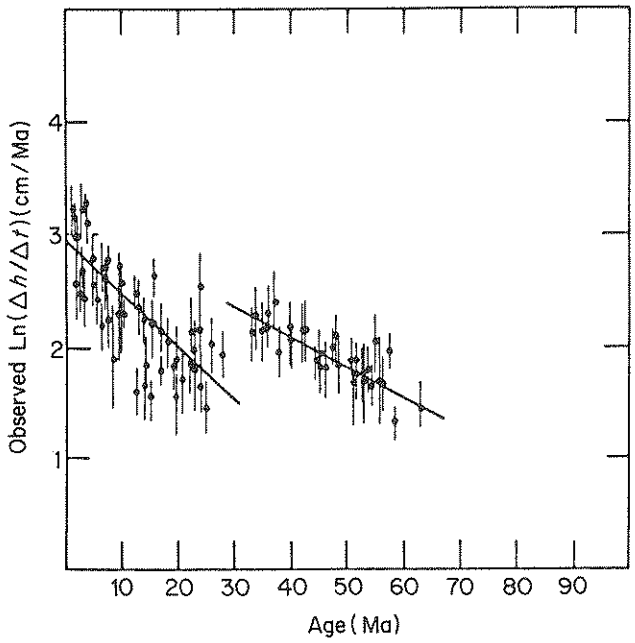

Fig. 10. Observed variation of the ratio of geoid offset to age offset ($\Delta h/\Delta t$) with increasing age.

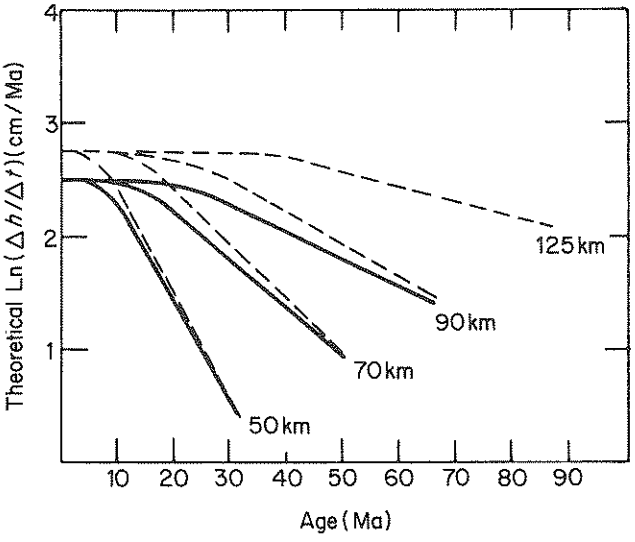

Fig. 11. Theoretical variations of Ln($\Delta h/\Delta t$) with age for the plate model, computed for several values of the thermal thickness H. Solid curves correspond to values of α, κ, T_m best-fitting the geoid data, while dashed curves correspond to values determined by Parsons and Sclater (1977); the top dashed curve, for $H = 125$ km, is their preferred model.

Turcotte (Chapter 5.4; Eqs. (43) and (48)) has developed the variation in geoid height $h(t)$ as a function of age t for both the half-space and plate models, due to thermal compensation associated with cooling and contraction of the oceanic lithosphere. The derivative $\Delta h/\Delta t$ of these expressions is easily derived. In the case of the half-space model, which predicts a linear decrease of the geoid height as age increases, the derivative is simply a constant. For the plate model, the geoid height is an exponentially decreasing function of age, and so is its derivative. The theoretical $\Delta h/\Delta t$ is shown in Fig. 11 in a semi-logarithmic plot in the case of the plate model, for two sets of the following thermal parameters: coefficient of thermal expansion, thermal diffusivity, bottom boundary temperature; and for four values of the thermal thickness. A comparison of Figs. 10 and 11 reveals that:

(i) the data show the linear decrease with age predicted by plate models, as long as t is not too small;
(ii) there exist two distinct linear trends, one characterizing the age range 0–30 Ma, the other the age range 30–60 Ma. A single set of thermal parameters cannot fit the whole dataset; rather, the two distinct trends could be explained by two distinct values of the plate thickness.

A least squares fit of the two groups of data gives a thermal thickness of ~65 km for the age range 0–30 Ma and ~95 km for the age range 30–60 Ma. These values appear significantly smaller than the value (~125 km) determined on the basis of depth to the sea floor (Parsons and Sclater, 1977). These results call for a number of remarks:

(i) geoid data across fracture zones appear incompatible with the half-space cooling model,
(ii) beyond 30 Ma, these data follow reasonably well the behavior predicted by the plate cooling model with a thermal thickness of ~95 km,
(iii) at younger ages, the data could still be interpreted in the context of the plate model with a thermal thickness of ~65 km but do not present the initial constant trend seen in the model curves (compare Figs. 10 and 11).

In view of these results, we are led to conclude that the plate model in its simplest version does not explain the geoid observations for young ages. Many reasons may be invoked. The apparent thinner thermal thickness for young lithosphere indicates that the bottom boundary isotherm of the plate is uplifted, a result of heat perturbations. If the geoid data considered above rise over large positive geoid anomalies associated with hot rising material of small-scale convection cells, we may thus invoke some heat perturbation. Other mechanisms should also be considered, in particular the possibility

hat the initial geotherm assumed in the plate model may not be an isotherm. Hot spots could represent another source of heat perturbation. This problem needs further investigation; in particular analyses of geoid data in other oceans would eventually help in clarifying the situation.

V. Use of Altimeter Data in Uncharted Marine Areas: Application to Bathymetric Prediction and Tectonic Reconstitutions

n some parts of the oceans, the spatial coverage of SEASAT exceeds that of surface-ship bathymetry. Altimeter derived geoid data have, therefore, been used to detect and predict bathymetry in uncharted regions. As we ave shown previously, each type of tectonic unit gives a specific response n the geoid and a systematic inspection of altimeter data has revealed the presence of numerous unsuspected seamounts, guyots, and in some cases of fracture zones and even subduction zones (e.g., Sailor and Okal, 1983; Ruff and Cazenave, 1985).

A. Seamounts

An example of the discovery of two uncharted seamounts from SEASAT data is shown on Figure 12 along the Louisville Ridge volcanic chain southeast Pacific). At geographical coordinates (37.5°S, 169.5°W) and 42.5°S, 163°W), the geoid points out to positive anomalies having characteristic seamount signatures in areas with extremely poor shipboard bathymetric coverage. Indeed, the discovery of new seamounts in oceanic areas has become very common since the advent of satellite altimetry (e.g. Lambeck and Coleman, 1982; Lazarewicz and Schwank, 1982; Dixon and Parke, 1983; Sandwell, 1984).

In the past 20 years, it has become apparent that our knowledge of he seamount population on the floor of the oceans is extremely poor. For example it took a strong volcanoseismic swarm to discover Macdonald Seamount (29°S, 140°W) in 1967, when its summit reached only 49 m below ea level (Johnson and Malahoff, 1971). Recently, Jordan *et al.* (1983) have used statistical techniques to extrapolate the known density of seamounts along linear shiptracks, and have revised the estimated density of seamounts n the Pacific by 1 to 2 orders of magnitude, suggesting that they make up as much as 0.4% of the oceanic crustal area, the great majority of them having yet to be discovered. It is clear that SEASAT-type altimetry can be

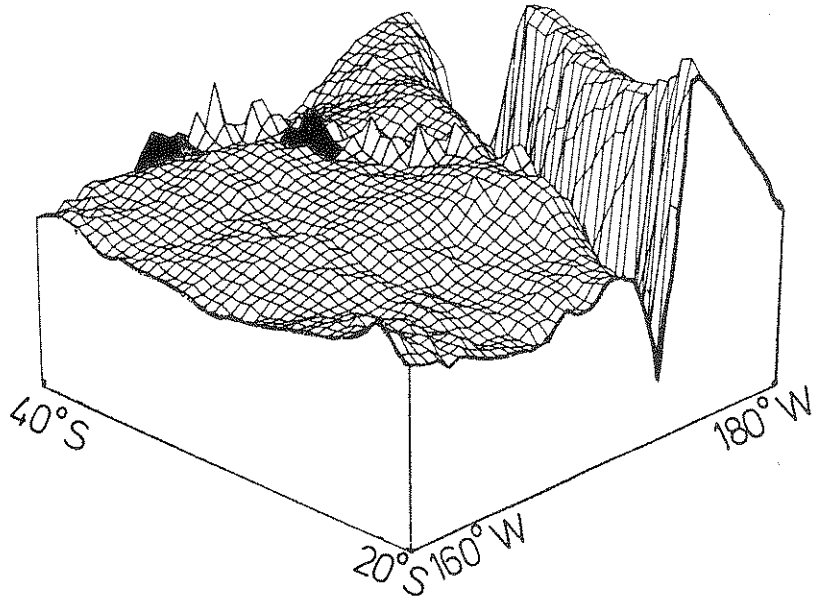

Fig. 12. Three-dimensional close-up of the geoid (with long wavelengths removed) in the area of the Tonga Trench, looking southwest, showing individual seamounts of the Louisville Ridge; the two seamounts shaded were discovered and identified by Cazenave and Dominh (1984).

of major help in starting to make inroads in this endeavor, and procedures have been developed for a systematic and automated scanning of SEASAT tracks for uncharted seamounts (e.g. White *èt al.*, 1983; Dixon *et al.*, 1983).

The interpretation of geoid signals in terms of the tectonic history of the associated bathymetric features is one of the major goals of their study; in the case of *seamounts*, the geoid response results from two opposite contributions: the positive effect of the topography plus the negative effect of its isostatic compensation. It has been found that the flexure of the lithosphere and geoid response to the loading depend critically on the age of the plate at the time of loading: an island or seamount formed on a very young portion of plate is supported only by a thin elastic layer ($H \leq 10$ km), and as a result literally sinks into the plate until substantial compensation is achieved. The resulting geoid signal is very weak if at all detectable. O the other hand, an island forming on sufficiently old (cooler) lithosphere is supported by a thicker elastic layer ($H \simeq 20$–30 km), resulting in only

partial isotatic compensation, and a strong geoid anomaly. Thus, the total observed geoid anomaly is smaller for seamounts formed "on-ridge" than for seamounts formed "off-ridge".

Therefore, and in order to predict bathymetry from altimetry in the case of a *previously uncharted seamount*, it is necessary to know the tectonic setting of the topography (i.e. age of the crust and age of the seamounts) as well as the relative density of the load and underlying mantle. Besides this problem of geophysical nature there is a severe problem of coverage of altimeter profiles. Where the satellite track passes adjacent to a seamount or in a saddle between two seamounts, a positive geoid anomaly is recorded which will of course be less than that produced by the actual bathymetry anomaly displaced off-track. Clearly, closely spaced ascending and descending profiles are needed to provide a valuable description of the topography.

Conversely, in the case of *charted seamounts or islands*, the concurrent knowledge of the geoid signature and of the bathymetry makes it possible to obtain the response function of the lithosphere to loading. Watts *et al.* (1980) have used this method to characterize a population of Pacific seamounts as generated either "off-ridge" or "on-ridge". In trying to model quantitatively the elastic response of the lithosphere to a seamount load, several problems arise: first from a methodological point of view, Cazenave and Dominh (1984) have shown that it is necessary to use real-life, two-dimensional modeling, rather than the linear, one-dimensional notion of admittance. Second, in interpreting the derived elastic thickness of the plate in terms of the age of the lithosphere upon formation of the seamount, it is necessary to take into account the effect of reheating (also known as "rejuvenation") of the plate by the mere presence of the magmatic edifice responsible for the island structure. This effect, originally proposed by Crough (1978) has been modeled, most recently by McNutt (1984), who has shown that, although the lithosphere bearing Hawaii is presently 80 Ma, it has the elastic properties of a 20 Ma plate. Similar numbers for Tahiti would be 75 and 15 Ma.

Nevertheless, it is usually possible to derive the basic character ("on-ridge" leading to full compensation, or "off-ridge", leading to elastic support) of an island or seamount for which geoid data and bathymetry are known. An example, taken from Okal and Cazenave (1985) is given in Fig. 13: the set of SEASAT tracks samples in a very similar fashion the flanks of the northern Tuamotu Islands (Tatakoto, Pukaruha) and southern Tuamotu Islands (Acteon, Marutea), as well as of the more recent Gambier chain. While the southern islands have a strong geoid signature, even at distances of 20–30 km, the northern ones are barely if at all detected. Quantification of these results led Okal and Cazenave to propose lithospheric ages of respectively 6–7 Ma and less than 2 Ma upon formation of

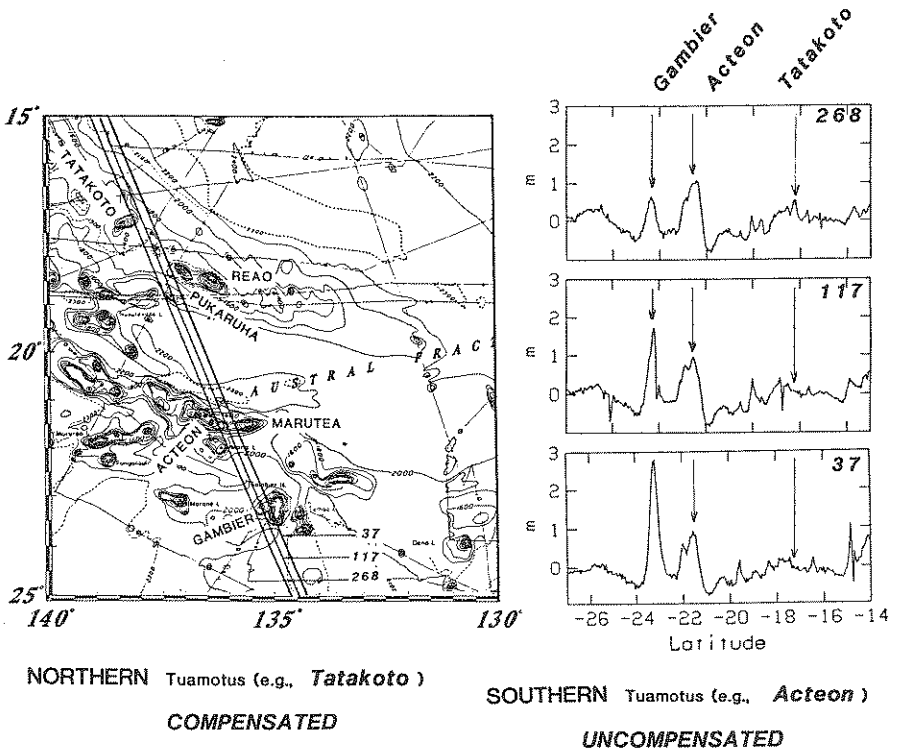

Fig. 13. Examples of compensated and uncompensated atolls in the Tuamotu Islands; see text for discussion. [After Okal and Cazenave (1985).]

the two chains. In the absence of igneous rocks allowing precise radiometric dating, such results are critical to the reconstruction of the tectonic history of oceanic atolls.

B. Fracture Zones

Although most major fracture zones have long been mapped on the basis of correlation of magnetic anomaly offsets, there remain areas of the ocean basins where improved knowledge of the topography of small fracture zones is necessary. Once again, the interpretation of SEASAT data has allowed complementary mapping of the extent of known fracture zones, as well as the discovery of new systems; Sailor and Okal (1983) and later Okal and Cazenave (1985) have used SEASAT data to infer the presence of two small fracture zones in the south central Pacific (see Fig. 14). These features, active about 25 Ma ago, were part of a short-lived pattern of spreading at the eastern boundary of the Pacific plate, which was then involved in an episode of ridge jump and reorientation, believed to be a possible consequence of the collision of North America with the Farallon Ridge. The transient nature of the fracture zone systems means that their present-day expression is confined to a small area, approximately 500×500 km^2, which had hitherto escaped shipboard detection; by using the models for $\Delta h/\Delta t$ described previously, Okal and Cazenave were able to estimate the age gap along these fracture zones. On the other hand, and more surprisingly, these authors have failed to identify the prolongation of a well-known nearby fracture zone (the Austral fracture zone) outside of its segment mapped from shipboard bathymetry (see Fig. 15). They proposed that an episode of rift propagation along the old Farallon ridge resulted in the transfer of the offset along the Austral fracture zone to the transient FZ1, as part of the process of evolution of the Farallon Ridge into the present-day East Pacific Rise.

C. Subduction Zones

As opposed to passive features, such as individual seamounts on the ocean floor or even fossil fracture zones, subduction zones are active agents in the motion of plates at the Earth's surface. It may then sound surprising that satellite altimeter data could be used to *discover and map* subduction zones, whose system should in principle be known.

However, in a recent study, Ruff and Cazenave have used SEASAT data to recognize the Hjort Trench, in the southernmost part of the Macquarie

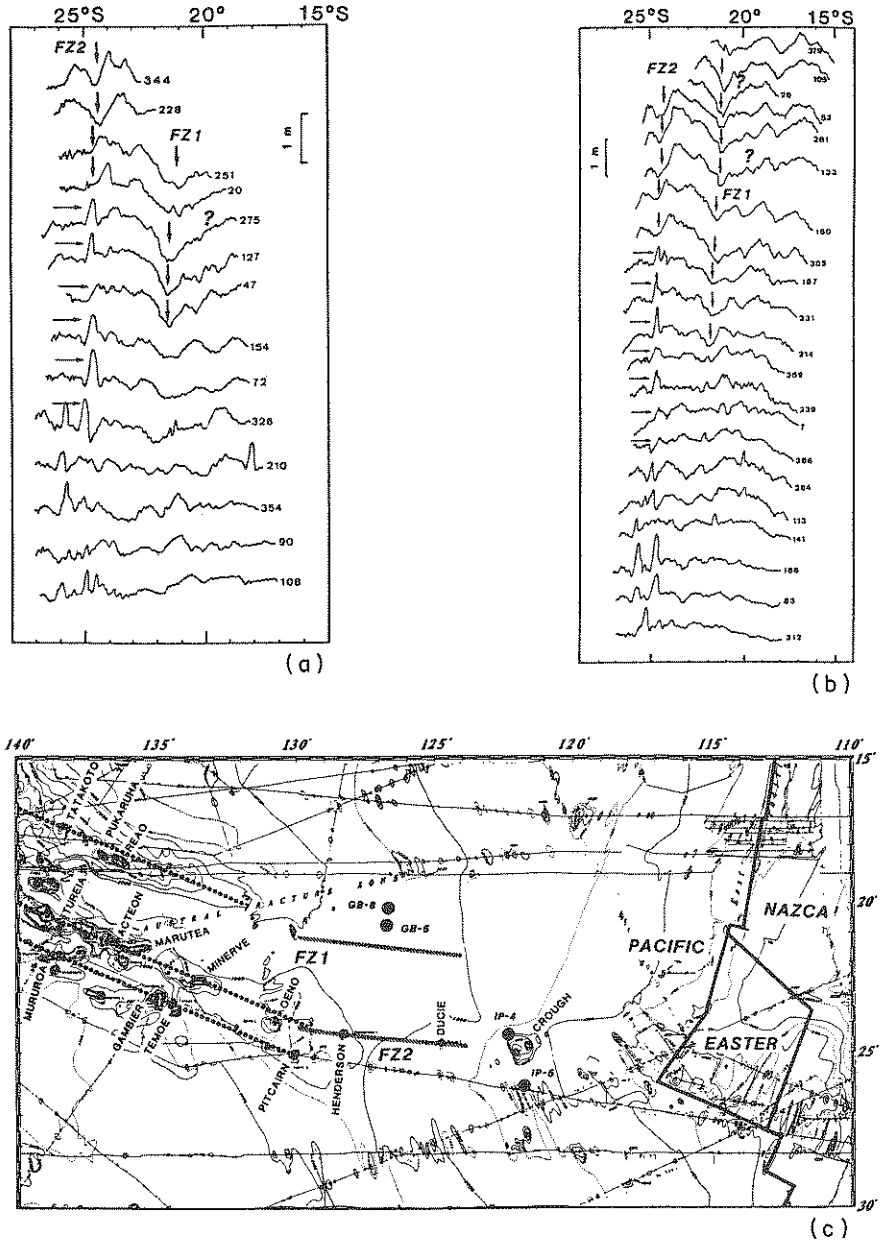

Fig. 14. Example of identification of uncharted tectonic features in the east central Pacific. Vertical arrows show fracture zones, horizontal ones seamounts. (a) Ascending profiles, (b) descending profiles and (c) map of area. [After Okal and Cazenave (1985).]

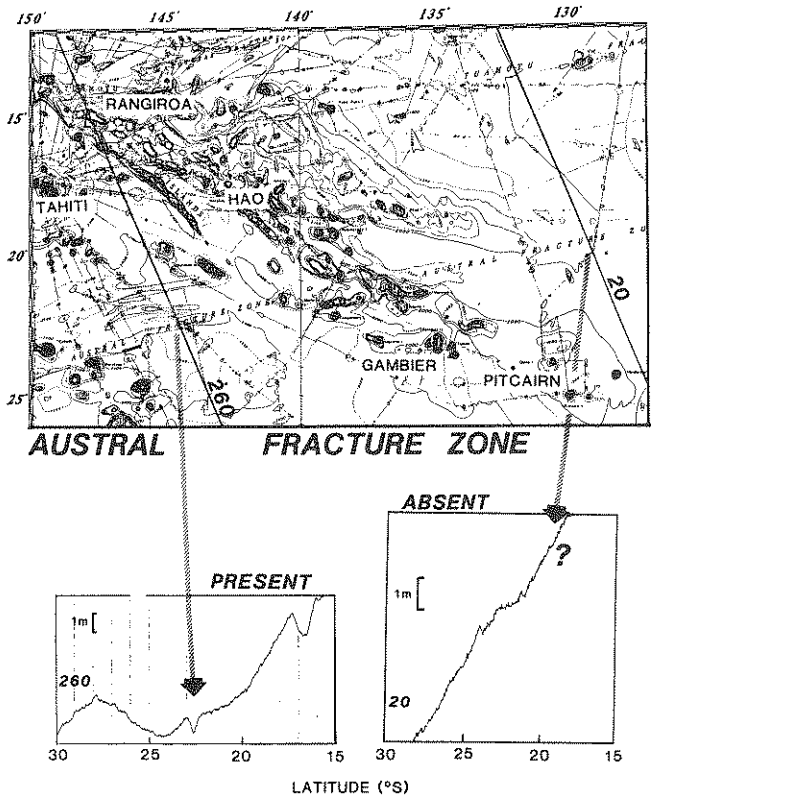

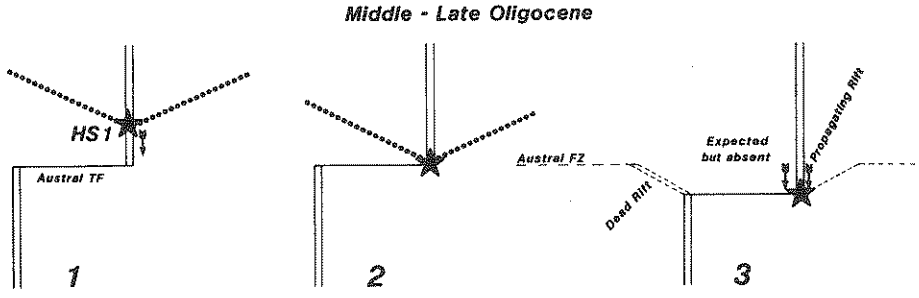

Fig. 15. Disappearance of Austral FZ signature east of 135° W. (top) Shipboard bathymetric map. (center) SEASAT data along tracks 20 and 260; arrows point from topographic location of crossing to corresponding point on SEASAT profile; note strong signal present on the western crossing, but absent from the eastern one (question mark), despite larger scale of figure. (bottom) Interpretation of the absence of the Austral fracture zone, as due to rift propagation of the Mendoza Ridge, upon interaction of the northern Tuamotu Hotspot (HS1) with the Austral transform fault.

Ridge complex, as involving subduction of the Australian plate under the Pacific one. Because of the proximity of this region to the pole of rotation of the two plates and of the generally poor shipboard bathymetry in the area, the exact nature and geometry of this plate boundary was not previously established. In addition to other partial seismic and marine evidence, altimeter data provide a conclusive proof that oblique subduction, rather than transform faulting, takes place at the southern part of the Macquarie Ridge. In particular, it provides the polarity of the subduction, showing that the Australian plate, rather than the Pacific one, is being subducted at the Hjort Trench (see Fig. 16).

The signature of the geoid in subduction zones depends obviously on the repartition of masses inside the Earth, and in particular on the stage of development and thermal state of the subducting slab. Thus, altimeter data can also be of great help to study zones where subduction is in the process of evolving: one such area is the northwestern coast of New Guinea, where the convergent component of the expected motion between Australia and the Pacific Plate is not released seismically (Kaplan and Seno, 1983; Okal *et al.*, 1983). The presence of a geoid signature comparable to that of subduction zones argues in favor of a dying or dead subduction zone, which may have existed as late as a few Ma ago (see Fig. 17).

On the other hand, the early stages of compressional deformation involved at the initiation of a new regime of subduction are carried out in the absence of a developed slab, and thus of a major density anomaly in the mantle; no large geoid height anomaly is expected. The area located between the Gilbert and Samoa Islands, where intense intraplate seismic activity has been recognized (Okal, 1984), but no significant geoid anomaly is present, may be undergoing the initial stages of the relocation of the Pacific-Australia plate boundary to the north of its present position (Okal *et al.*, 1986). A more developed stage, where subduction has clearly started, but the geoid signature lacks the characteristic trough present at mature trenches, is the Puysegur Trench, just south of New Zealand, at the northern end of the Macquarie system (see Fig. 16).

V. Conclusion

Satellite altimeters have given us coverage of the geoid at wavelengths which were previously inaccessible on a worldwide basis. As we have detailed before, a wealth of new geophysical results have been obtained. When combined with bathymetric knowledge, geoid data provide constraints on the Earth's elastic response and, thus, on the cooling processes of the oceanic lithosphere. On the other hand, in the absence of adequate bathymetric

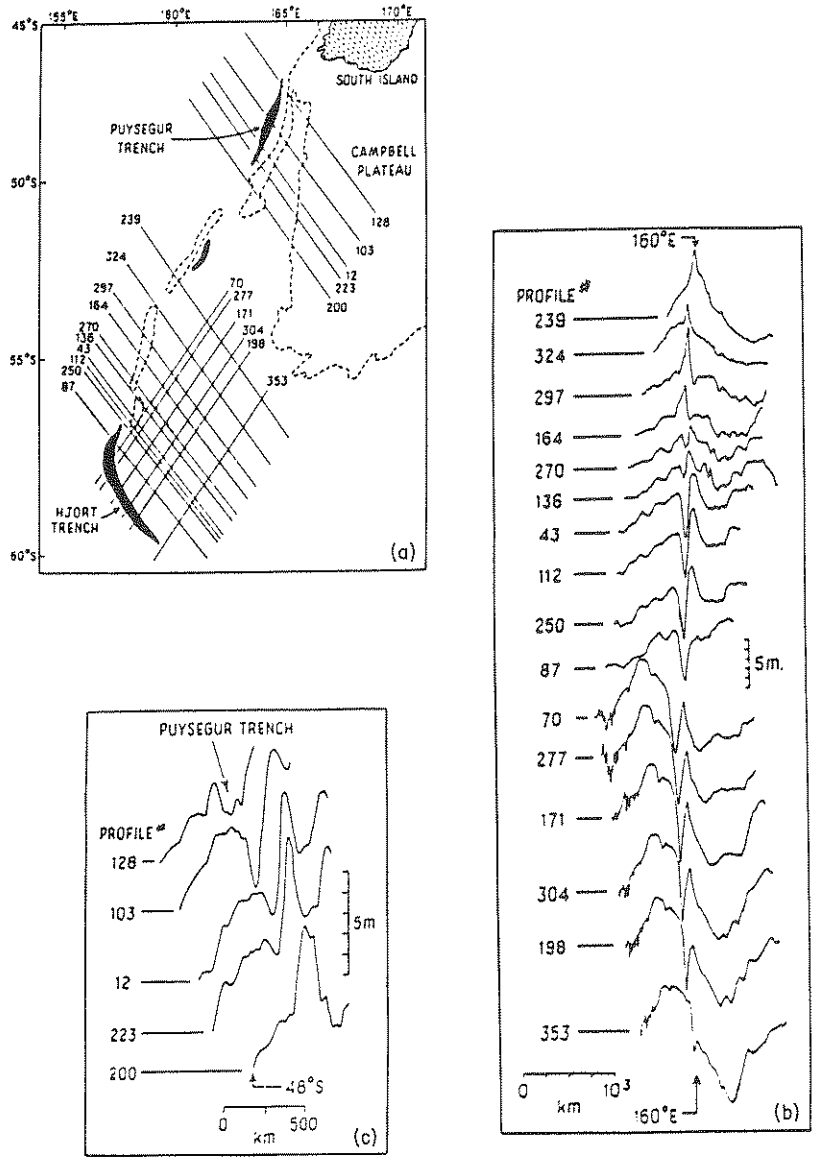

Fig. 16. (a) Index map of SEASAT profiles used in the Macquarie region. Trenches are identified by the 2600-fathom contour and the dashed lines show the 1000-fathom contour. (b) SEASAT profiles across the Hjort Trench region. Note the definite trough present on profiles 43, 112, 250, 87 and the outer rise on tracks 70 and 277. (c) SEASAT profiles across the Puysegur Trench. Note absence of the 5-m deep-trough characteristic of mature subduction and present at the Hjort Trench. [After Ruff and Cazenave (1985).]

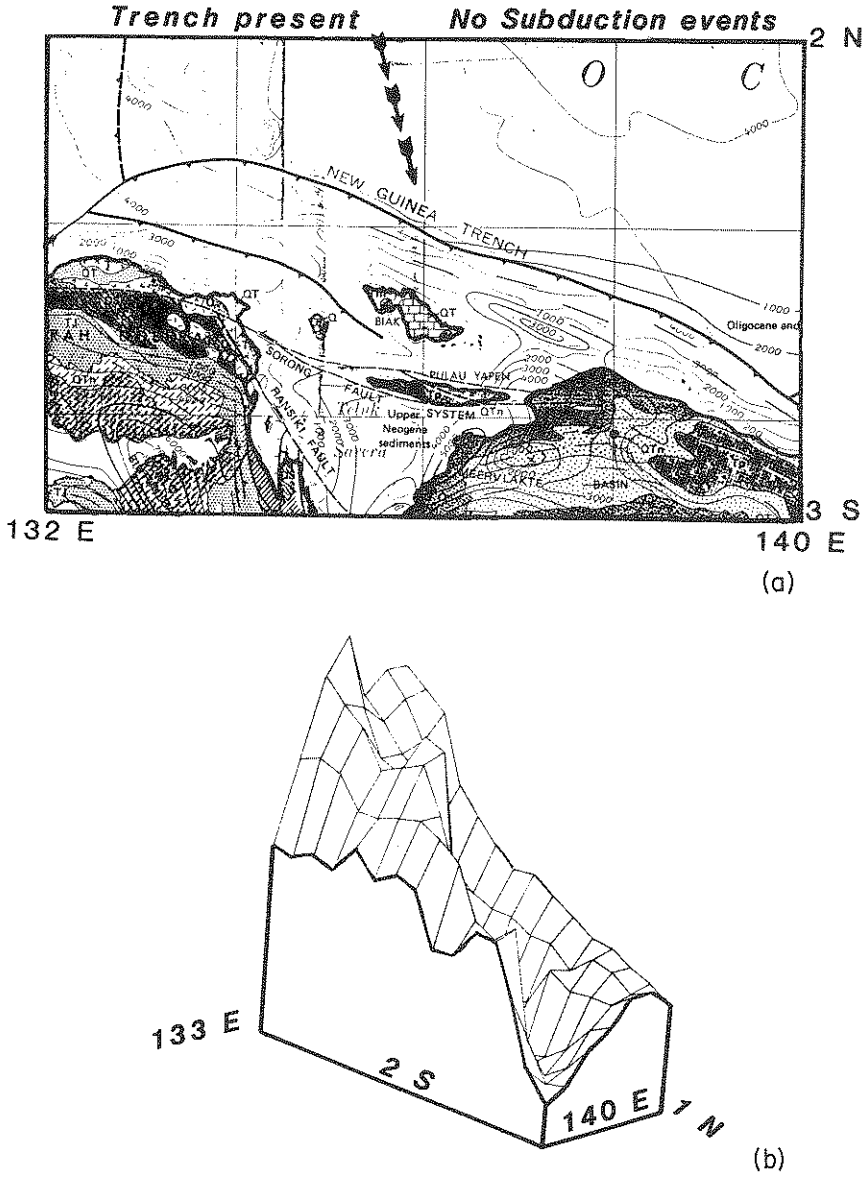

Fig. 17. (a) Tectonic map of northwestern New Guinea (After Hamilton, 1979), showing bathymetric expression of "New Guinea Trench", deeper than 5000 m, but lacking subduction earthquakes. (b) Three-dimensional view of geoid anomalies (long wavelengths removed) in New Guinea trench area, showing trough characteristic of subduction systems, and suggesting "dead" subduction zone.

coverage, satellite altimetry is the most efficient way of mapping uncharted tectonic features. Several problems of importance to present-day plate tectonics have been solved through this technique.

These results are all the more encouraging in the view of the untimely failure of the SEASAT mission after only 105 days in orbit, which resulted in uneven and occasionally sparse gridding of the ocean surface. This in turn has hampered efforts aimed at systematic bathymetric prediction. It would be highly desirable that future planning of altimeter missions be designed to fill the gaps between existing profiles, at least over selected oceanic regions.

References

Balmino, G., Brossier, C., Cazenave, A., Dominh, K., Nouel, F. and Vales, N. (1979). Geoid of the Kerguelen Islands area determined from GEOS-3 altimeter data. *J. Geophys. Res.* **84**, 3827–3831.

Bottinga, Y. (1974). Thermal aspects of sea-floor spreading, and the nature of the suboceanic lithosphere. *Tectonophysics* **21**, 15–38.

Bottinga, Y. and Allègre, C. J. (1976). Geophysical, petrological and geochemical models of the oceanic lithosphere. *Tectonophysics* **32**, 9–59.

Cazenave, A. (1984). Thermal cooling of the oceanic lithosphere: new constraints from geoid height data. *Earth Planet. Sci. Lett.* **70**, 395–406.

Cazenave, A. and Dominh, K. (1984). Geoid heights over the Louisville Ridge (South Pacific). *J. Geophys. Res.* **89**, 11171–11179.

Crough, S. T. (1978). Thermal origin of mid-plate hotspot swells. *Geophys. J. R. Astron. Soc.* **55**, 451–469.

Dixon, T. H. and Parke, M. E. (1983). Bathymetry estimates in the southern oceans from SEASAT altimetry. *Nature* **304**, 406–411.

Hamilton, W. (1979) Tectonics of the Indonesian Region. *U.S. Geol. Surv. Prof. Pap.* **1078**.

Heestand, R. L. and Crough, S. T. (1981). The effect of hotspots on the oceanic age-depth relation. *J. Geophys. Res.* **86**, 6107–6114.

Johnson, R. H. and Malahoff, A. (1971). Relationship of Macdonald Volcano to migration of volcanism along the Austral Chain. *J. Geophys. Res.* **76**, 3282–3290.

Jordan, T. H., Menard, H. W. and Smith, D. K. (1983). Density distribution of seamounts in the eastern Pacific inferred from wide-beam sounding data. *J. Geophys. Res.* **88**, 10508–10518.

Kaplan, D. A. and Seno, T. (1983). Seismotectonics of western New Guinea. *EOS, Trans. Am. Geophys. Un.* **63**, 1023 (abstract).

Lambeck, K. (1981). Lithospheric response to volcanic loading in the southern Cook islands. *Earth Planet. Sci. Lett.* **55**, 482–496.

Lambeck, K. and Coleman, R. (1982). A search for seamounts in the southern Cook and Austral region. *Geophys. Res. Lett.* **9**, 389–392.

Lazarewicz, A. R. and Schwank, D. C. (1982). Detection of uncharted seamounts using satellite altimetry. *Geophys. Res. Lett.* **9**, 385–388.

Lerch, F. J., Putney, B. H., Wagner, C. A. and Klosko, S. M. (1981). Goddard Earth models for oceanographic applications. *Mar. Geod.* **4**, 145–187.

Marsh, B. D., Marsh, J. G. and Williamson, R. G. (1984). On Gravity from SST, geoid from SEASAT, and plate age and fracture zones in the Pacific. *J. Geophys. Res.* **89**, 6070–6078.

Marsh, J. G., Martin, T. V., McCarthy, J. J. and Chovitz, P. S. (1980). Mean sea surface computation using GEOS-3. *Mar. Geod.* **3**, 359–378.

Marsh, J. G., Cheney, R. E., McCarthy, J. J. and Martin, T. V. (1985). Regional mean sea surfaces based upon GEOS-3 and SEASAT. *Mar. Geod.* **8**, 385–402.

Marsh, J. G., Brenner, A. C., Beckley, B. D. and Martin, T. V. (1986). Global mean sea surfaces based upon the SEASAT altimeter data. *J. Geophys. Res.* **91**, 3501–3506.

McKenzie, D. P. (1967). Some remarks on heat flow and gravity anomalies. *J. Geophys. Res.* **72**, 6261–6273.

McKenzie, D. P., Watts, A. B., Parsons, B. and Roufosse, M. (1980). Planform of mantle convection beneath the Pacific Ocean. *Nature* **288**, 442–446.

McNutt, M. K. (1984). Lithospheric flexure and thermal anomalies. *J. Geophys. Res.*, **89**, 11180–11194.

Okal, E. A. (1984). Intraplate Seismicity of the southern part of the Pacific plate. *J. Geophys. Res.* **89**, 10053–10071.

Okal, E. A., and Cazenave, A. (1985). A model for the plate tectonics evolution of the east central Pacific based on SEASAT investigations. *Earth Planet. Sci. Lett.* **72**, 99–117.

Okal, E. A., Woods, D. F. and Lay, T. (1986). Intraplate deformation in the Samoa–Gilbert–Ralik area: a prelude to a change of plate boundaries in the South Pacific? *Tectonophysics* (in press).

Okal, E. A., Heineman, M. and Grall, H. M. (1983). Tectonic implications of the seismicity of northwestern New Guinea, 1910–1979. *EOS, Trans. Am. Geophys. Un.* **64**, 265 (abstract).

Oldenburg, D. W. (1975). A physical model for the creation of the lithosphere. *Geophys. J. R. Astron. Soc.* **43**, 425–451.

Parker, R. L., and Oldenburg, D. W. (1973). Thermal models of ocean ridges. *Nat. Phys. Sci.* **242**, 137–139.

Parsons, B. and Richter, F. M. (1980). A relation between the driving force and geoid anomaly associated with mid-ocean ridges. *Earth Planet. Sci. Lett.* **51**, 445–450.

Parsons, B., and Sclater, J. G. (1977). An analysis of the variation of ocean floor bathymetry and heat flow with age. *J. Geophys. Res.* **82**, 803–827.

Rapp, R. H. (1983). The determination of geoid undulations and gravity anomalies from SEASAT altimeter data. *J. Geophys. Res.* **88**, 1552–1562.

Reigber, C., Muller, H., Bosch, W., Balmino, G. and Moynot, B. (1985). GRIM gravity model improvement using LAGEOS. *J. Geophys. Res.* (submitted).

Ruff, L. J. and Cazenave, A. (1985). SEASAT geoid anomalies and the Macquarie Ridge complex. *Phys. Earth Planet. Inter.* **38**, 59–69.

Sailor, R. V. and Okal, E. A. (1983). Application of SEASAT data in seismotectonic studies of the south central Pacific. *J. Geophys. Res.* **88**, 1572–1580.

Sandwell, D. T. (1984). A detailed view of the South Pacific geoid from satellite altimetry. *J. Geophys. Res.* **89**, 1089–1104.

Sandwell, D. T. and Schubert, G. (1980). Geoid height versus age for symmetric spreading ridges. *J. Geophys. Res.* **85**, 7235–7241.

Sclater, J. G. and Francheteau, J. (1970). The implications of terrestrial heat flow observations on current tectonic and geochemical models of the crust and upper mantle of the Earth. *Geophys. J. R. Astron. Soc.* **20**, 509–542.

Turcotte, D. L. and Oxburgh, E. R. (1967). Finite amplitude convective cells and continental drift. *J. Fluid Mech.* **28**, 29–42.

Vening Meinesz, F. A. (1941). Gravity over the Hawaiian archipelago and over the Madiera area: conclusions about the Earth's crust. *Proc. Kon. Ned. Akad. Wetensch.*

Watts, A. B. (1978). An analysis of isostasy in the world's oceans, 1. Hawaiian-Emperor seamount chain. *J. Geophys. Res.* **83**, 5989-6004.

Watts, A. B., Bodine, J. H. and Ribe, N. M. (1980). Observations of flexure and the geological evolution of the Pacific Ocean basin. *Nature* **283**, 532-537.

Watts, A. B., Karner, G. D. and Steckler, M. S. (1982). Lithospheric flexure and the evolution of sedimentary basins. *Phil. Trans. R. Soc. London, A* **305**, 249-281.

Watts, A. B., McKenzie, D. P., Parsons, B. and Roufosse, M. (1985). The relationship between gravity and bathymetry in the Pacific Ocean. *Geophys. J. R. Astron. Soc.* **83**, 263-298.

White, J. V., Sailor, R. V., Lazarewicz, A. R. and LeSchack, A. R. (1983). Detection of seamount signatures in SEASAT altimeter data using matched filters. *J. Geophys. Res.*, **88**, 1541-1551.

Wood, B. J. and Yuen, D. A. (1983). The role of lithospheric phase transitions on seafloor flattening at old ages. *Earth Planet. Sci Lett.* **66**, 303-314.